Journal of Hepatocellular Carcinoma

Dovepress
Taylor & Francis Group

Open Access Full Text Article

ORIGINAL RESEARCH

Preoperative Prediction of Macrotrabecular-Massive Hepatocellular Carcinoma Using Machine Learning-Based Ultrasomics

Yahong Li[1], Shaobo Duan[2], Shanshan Ren[3], Dujuan Li[4], Yujing Ma[5], Didi Bu[1], Yuanyuan Liu[1], Xiaoxiao Li[5], Xiguo Cai[6], Lianzhong Zhang[1,3]

[1]Department of Ultrasound, Zhengzhou University People's Hospital, Henan Provincial People's Hospital, Henan, People's Republic of China; [2]Department of Health Management, Henan Provincial People's Hospital, Henan, People's Republic of China; [3]Department of Ultrasound, Henan Provincial People's Hospital, Henan, People's Republic of China; [4]Department of Pathology, Henan Provincial People's Hospital, Henan, People's Republic of China; [5]Department of Ultrasound, Henan University People's Hospital, Henan Provincial People's Hospital, Henan, People's Republic of China; [6]Department of Rehabilitation, Henan Rehabilitation Clinical Medical Research Center, Henan Provincial People's Hospital, Henan, People's Republic of China

Correspondence: Lianzhong Zhang, Department of Ultrasound, Henan Provincial People's Hospital, No. 7, Weiwu Road, Jinshui District, Zhengzhou City, Zhengzhou, 450003, People's Republic of China, Tel +86-371-87160869, Email zlz8777@163.com

Purpose: Macrotrabecular-massive hepatocellular carcinoma (MTM-HCC) is a special pathological subtype of HCC, which is related to invasiveness and poor prognosis. We aimed to construct an ultrasomics model for preoperative noninvasive prediction of MTM-HCC.

Patients and Methods: Patients with pathologically confirmed HCC who underwent liver surgery between January 2021 and December 2023 were retrospectively enrolled. 211 eligible patients (169 males and 42 females) were divided 7:3 into the training set (n=147) and test set (n=64) by random stratified sampling. Ultrasomics models were constructed based on the ultrasound image features of the training set using five different ML algorithms, including random forest (RF), eXtreme gradient boosting (XGBoost), support vector machine (SVM), decision tree (DT), and logistic regression (LR). Additionally, a model based on clinical features and a combined model based on clinical and ultrasomics features were constructed to predict MTM-HCC. The performance of the models in the preoperative prediction of MTM-HCC was evaluated on the test set using area under the receiver operating characteristic curve (AUC), sensitivity, specificity, and accuracy.

Results: The ultrasomics models and the combined models of the five algorithms were effective in predicting MTM-HCC, and the combined models have improved AUC after adding clinical features compared with the ultrasomics model in the test set. The model constructed based on the RF algorithm in the test set has a high accuracy rate and specificity, and the overall performance of the models is better than that of the other four algorithm models, the AUC, accuracy, specificity, and sensitivity of its combined model and ultrasomics model are significantly higher than the clinical model.

Conclusion: ML-based ultrasomics model is an effective tool for predicting MTM-HCC before surgery. Integrating clinical and ultrasound image features enhances predictive performance, offering a novel approach for non-invasive preoperative diagnosis of MTM-HCC.

Keywords: prediction, aggressiveness, macrotrabecular-massive subtype, ultrasomics

Introduction

Hepatocellular carcinoma (HCC) is the most prevalent form of primary liver cancer, representing about 75–85% of cases and ranking as the third leading cause of cancer deaths globally.[1] Despite significant advances in HCC treatment, the overall prognosis of HCC remains poor,[2] largely due to the potential genetic alterations, molecular characteristics, and

Received: 24 November 2024
Accepted: 28 March 2025
Published: 12 April 2025

histological patterns.[3] According to the fifth edition of the World Health Organization classification of tumors in 2019, approximately 35% of HCCs are special pathological subtypes, including steatohepatitic, clear cell type, MTM, scirrhous, chromophobe, fibrolamellar, neutrophil-rich, and lymphocyte-rich subtypes.[4] Recent reports have shown that MTM-HCC is an invasive HCC subtype[5–7] closely associated with TP53 gene mutations, fibroblast growth factor 19 (FGF19) amplification, and the ataxia -telangiectasia mutated (ATM) protein.[8] Meanwhile, this subtype is an independent predictor of early and overall recurrence in patients who have undergone surgical resection[9] and is linked to poor clinical prognosis.[5,10] Liu et al reported high PD-L1 expression in the MTM-HCC subtype, suggesting that patients with MTM-HCC may benefit from tumor immunotherapy.[11] Accurate preoperative diagnosis of MTM-HCC is of great significance to the choice of clinical treatment methods and the improvement of prognosis. Although pathological examination can accurately diagnose MTM-HCC before operation, there are risks such as invasiveness, sampling error, and possible complications. Therefore, a non-invasive, simple and reproducible examination method is urgently needed to help clinical preoperative diagnosis of MTM-HCC.

Radiomics is an emerging technology that enables the high-throughput extraction of medical image features, followed by the selection of key features using dimensionality reduction, to construct models for evaluating information related to diagnosis, treatment response and prognosis of oncological diseases.[12–17] For example, Hawkins et al found that RF classification-based CT imaging can be used to predict the occurrence of lung cancer nodules.[12] The peritumor vascular and intratumoral radiomics model developed by Xie et al provided a non-invasive tool to predict pathologic complete responses in triple-negative breast cancer patients receiving neoadjuvant chemoradiotherapy.[13] Regarding the application of radiomics to predict MTM-HCC, there have been preliminary studies in the direction of CT and, MRI,[18–20] and achieved good prediction results. For example, Feng et al collected contrast-enhanced CT image data and developed an SVM-based radiomics model based on the training set. The authors found that the AUCs of the model in the training set, internal test set, and external test set were 0.84, 0.80, and 0.74, respectively.[18]

However, compared with CT and MRI, ultrasound is simple, radiation-free, portable and lower cost. In recent years, AI-driven ultrasound technology has been further developed and applied in clinical practice to reduce subjectivity and improve the efficiency of ultrasound diagnosis,[21] and many studies have confirmed its value in liver diseases. Peng et al used dimensionality reduction techniques and machine learning methods to develop ultrasonomics models that can be used to predict HCC, intrahepatic cholangiocarcinoma and combined hepatocellular-cholangiocarcinoma in preoperative noninvasive differentiation.[22] Ren et al constructed an SVM-based algorithm to construct an ultrasomics model that can be used to help in preoperative noninvasive prediction of HCC pathological grade.[23] Dong et al[24] published a study that the SVM algorithm based on grayscale ultrasound images has the potential to help predict preoperative microvascular invasion status in HCC. However, the accuracy of ultrasomics in the preoperative prediction and differential diagnosis of MTM-HCC is currently unclear. This study developed different ultrasomics models using ML to predict MTM-HCC before surgery, offering a new approach for non-invasive, early diagnosis and treatment selection for the disease.

Material and Methods

Subjects

This retrospective study was approved by the Medical Ethics Committee of Henan Provincial People's Hospital (2021 Ethics Review No. 01) and exempted the patient from informed consent.

From January 2021 to December 2023, Patients with pathologically confirmed HCC were enrolled consecutively. The detailed eligibility criteria were as follows:

Inclusion criteria: (1) pathologically confirmed hepatocellular carcinoma, with complete pathological data; (2) abdominal ultrasound performed two weeks before surgery, with available ultrasound images; (3) underwent radical resection for liver cancer. Exclusion criteria: (1) prior radiotherapy, chemotherapy, radiofrequency ablation or other antitumor treatments; (2) other comorbid malignancies; (3) Patients with unclear ultrasound images and incomplete lesion display; (4) lack of complete clinical pathological data. Finally, 211 patients were enrolled in the study. The case screening process is shown in Figure 1.

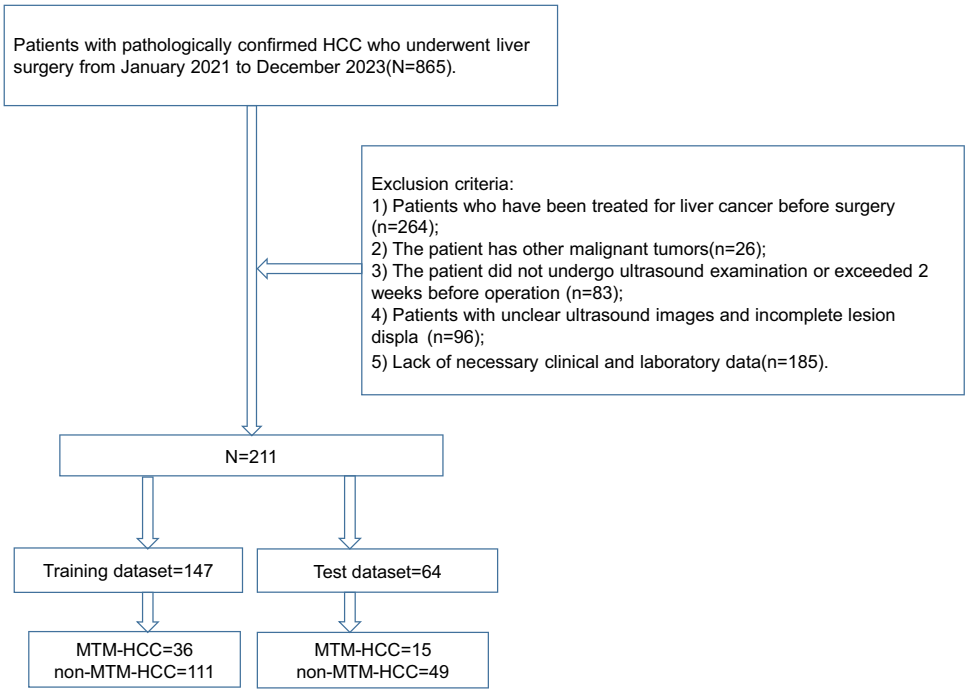

Figure 1 Screening and enrollment of cases according to established eligibility criteria.

Clinical Data

Clinical data that were collected included age, sex, history of hepatitis, cirrhosis, splenomegaly, ascites, portal hypertension, tumor biomarker (alpha-fetoprotein, AFP), aspartate aminotransferase (AST), alanine aminotransferase (ALT), albumin (ALB), globulin (GLO), albumin-globulin ratio (A/G), total bilirubin (TBIL), direct bilirubin (DBIL), indirect bilirubin (IBIL), alkaline phosphatase (ALP), creatinine (CREA), activated partial thromboplastin time (APTT), prothrombin activity (PTA), prothrombin time (PT), fibrinogen (FIB), and thrombin time (TT).

Pathological Data

All histological sections were reviewed by a senior pathologist who was unaware of the patients' clinical and imaging data. MTM-HCC was defined as tumors with a macrotrabecular growth pattern (trabeculae more than six cells thick) observed in more than 50% of the tumor tissue according to histologic diagnostic criteria.[25]

Image Acquisition and Segmentation

Patients were required to fast for more than 8 hours before examination. Each patient was examined by ultrasonographers with more than 10 years of experience, and ultrasound images were saved in Digital Imaging and Communications in Medicine (DICOM) format. To reduce sample selection bias, the largest lesion was selected as the target lesion for patients with multiple lesions. Ultrasound images showing the largest diameter of the target lesion were analyzed. The model of ultrasound instrument used in the examination: GE Logiq E20, GE Vivid E9, Philips EPIQ 7, HIVISION Ascendus, etc. Choose convex array abdominal probe with frequency of 1–5MHz.

To minimize differences between ultrasound equipment and operators and to facilitate subsequent feature extraction and comparison, images were preprocessed by researchers with eight years of experience. During the preprocessing stage, first, image features were standardized using the z-score. Second, the interpolation resampling method was applied to achieve a pixel size of 1mm × 1 mm using B-spline interpolation. The image is grayscale discretized in the histogram, with the bin width fixed at 25, and then feature calculation is performed.

Image segmentation was performed using the open-source software ITKSNAP (http://www.itksnap.org). The region of interest (ROI), was first delineated manually by an ultrasound doctor with 15 years of experience in ultrasound. Thirty

randomly selected target lesions were delineated independently by another ultrasound doctor (with 30 years of experience). The intraclass correlation coefficient (ICC) assessed intra-observer consistency, with an ICC≥0.8 indicative of reproducibility.[26] A flowchart of the study procedure is shown in Figure 2.

Feature Extraction and Selection

The original images apply 14 filters to obtain the derived images for each patient. Feature extraction was performed on all original and derived images using Pyradiomics. The extracted features mainly included first-order statistical features, two-dimensional shapes, gray level co-occurrence matrix (GLCM), gray level run length matrix (GLRLM), gray level size zone matrix (GLSZM), neighborhood gray-tone difference matrix (NGTDM), and gray level dependence matrix (GLDM). Dimensionality reduction was performed on the features using a combination of variance filtering, mutual information, and the embedding method combined with XGBoost to reduce redundant features and improve modeling efficiency and model accuracy.

Model Construction and Evaluation

Data were divided 7:3 into a training set (n=147) and a test set (n=64) using a stratified sampling method. The screened ultrasound image features were used to construct ultrasomics model. Univariate and multivariate analyses were adopted to screen out statistically significant factors from the clinical data, and constructed clinical model. A combined model was built by integrating both clinical features and ultrasomics features. Five ML algorithms, namely RF, XGBoost, SVM, DT, and LR, were each used to construct the three models for the training set. The performance of the models was evaluated on the test set using AUC, sensitivity, specificity, and accuracy. The working steps are presented in the form of pseudo-code in Figure 3.

Statistical Analysis

Data were analyzed using IBM SPSS Statistics 27.0. Quantitative data are expressed as mean ± standard deviation when normally distributed, and as median (interquartile range) when not normally distributed. These data were compared between groups using the independent *t*-test or Mann–Whitney *U*-test. Qualitative data are expressed as numbers(percentages) and compared using the Chi-square test or Fisher's exact test. $P < 0.05$ was considered statistically significant.

Results

Clinical and Pathological Features

Of the 211 patients included in this study, 169 were males and 42 were females, with an age of 28–85 years (57.36 ± 10.05 years). Among them, 51 cases (24.2%) were diagnosed with MTM-HCCs and 160 cases (75.8%) with non-MTM-

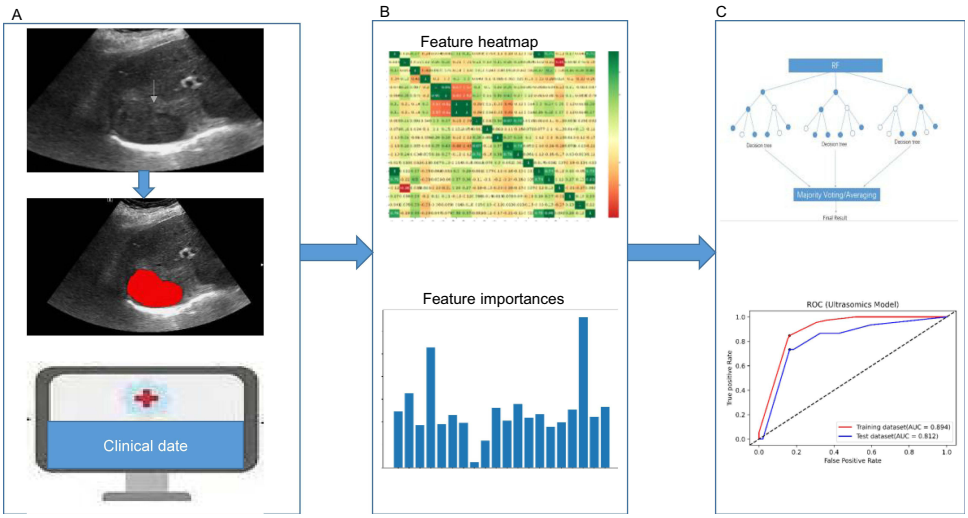

Figure 2 Overall study flow chart. (**A**) Image acquisition and lesion segmentation (**B**) Feature extraction and selection (**C**) Model construction and evaluation.

Algorithm 1 Model Training and Evaluation

Input: 211 samples in total, including 51 positive samples and 160 negative samples.
Output: combined model, ultrasomics model, and clinical model

Process the sample data through preprocessing and feature engineering into combined data D_1, ultrasomics data D_2, clinical data D_3
for each $Di \in \{D_1, D_2, D_3\}$ **do**
  Di were divided 7:3 into training set D_{i_train} and test set D_{i_test} using stratified sampling method
end for
Initialize machine learning algorithm $A = \{\mathrm{RF}, \mathrm{XGBoost}, \mathrm{SVM}, \mathrm{DT}, \mathrm{LR}\}$
for each $(d_{train}, d_{test}) \in \{(D_{1\_train}, D_{1\_test}), (D_{2\_train}, D_{2\_test}), (D_{3\_train}, D_{3\_test})\}$ **do**
  Initialize Evaluation indicator threshold $\tau \leftarrow$ Default value
  repeat
    for each algorithm $a \in \mathcal{A}$ **do**
      Train model M_a on dataset d_{train} using algorithm a
      Calculate performance indicators on d_{test} :
        $\mathrm{AUC}_a, \mathrm{sensitivity}_a, \mathrm{specificity}_a, \mathrm{accuracy}_a$
      if $\mathrm{AUC}_a, \mathrm{sensitivity}_a, \mathrm{specificity}_a, \mathrm{accuracy}_a \geq \tau$ **then**
        $M \leftarrow \mathrm{Ensemble}(\{M_a\})$ ▷ Integrate all the models that meet the standards
        break
      end if
    end for
  until M achieves the expected effect
end for
return $M_{combined}$, $M_{ultrasomics}$, $M_{clinical}$

Figure 3 The pseudo-code corresponding to the algorithm is shown in Algorithm 1.

HCCs. There were no noticeable difference between the training set and test set. The baseline clinical and pathological data of the patients are shown in Table 1. Univariate analysis revealed that ALT (P=0.017), AST (P<0.001), AFP (P=0.005), gender (P=0.038), and tumor diameter (P<0.001) were statistically significant between MTM-HCC and non-MTM-HCC groups, as shown in Table 2. The relevant factors were incorporated into a multivariable logistic regression analysis, with results shown in Table 3. The findings indicate that higher levels of AFP (P=0.031), AST (P=0.030), and tumor diameter (P=0.034) are independent risk factors for diagnosing MTM-HCC. The ultrasound images and histological patterns of non-MTM-HCC and MTM-HCC are shown in Figure 4.

Table 1 Clinical and Pathological Data of Patients in Training Set and Test Set

Characteristic	Training Set (n=147)	Test Set (n=64)	*P* Value
Gender			0.075
Male	113 (76.9%)	56 (87.5%)	
Female	34 (23.1%)	8 (12.5%)	
Age (years)	57.28 (±10.16)	57.56(±9.86)	0.851
HbsAg/HCV Ab			0.621
Positive	106(72.1%)	44 (68.8%)	
Negative	41(27.9%)	20 (31.2%)	
Cirrhosis			0.542
Yes	118(80.3%)	49(76.6%)	
No	29(19.7%)	15(23.4%)	
Splenomegaly			0.227
Yes	73(49.7%)	26(40.6%)	
No	74(50.3%)	38(59.4%)	
Ascites			0.412
Yes	21 (14.3%)	12 (18.8%)	
No	126 (85.7%)	52 (81.2%)	
Portal hypertension			0.928
Yes	63 (42.9%)	27 (42.2%)	
No	84 (57.1%)	37 (57.8%)	

(*Continued*)

Table 1 (Continued).

Characteristic	Training Set (n=147)	Test Set (n=64)	*P* Value
ALT (U/L)	29.7 (20.8, 51.0)	31.2 (16.8, 51.9)	0.894
AST (U/L)	32.5 (23.2, 43.1)	34.7 (24.3, 55.0)	0.433
ALB (g/L)	36.8 (36.5, 42.8)	39.6 (36.6, 42.9)	0.977
GLO (g/L)	27.1 (24.2, 31.0)	28.2 (25.1, 31.2)	0.277
A/G	1.5(±0.33)	1.4(±0.32)	0.545
TB (umol/L)	13.0 (9.2, 19.5)	12.9 (9.4, 17.5)	0.886
DB (umol/L)	4.0 (3.1, 5.5)	4.1 (3.2, 6.1)	0.441
IB (umol/L)	8.9 (6.2, 12.9)	8.7 (5.8, 11.3)	0.561
ALP (U/L)	85.3 (67.6, 110.9)	83.4 (68.9, 103.7)	0.593
CREA (umol/L)	62 (53.0, 69.0)	64.5 (55.3, 74.8)	0.088
PT (S)	12.4 (11.7, 13.1)	12.4 (11.6, 13.0)	0.634
PTA (%)	92.3 (86.1, 99.1)	92.3 (87.2, 100.0)	0.625
APTT (S)	27 (26.0, 29.1)	27.5 (25.8, 28.8)	0.738
FIB (g/L)	2.5 (2.0, 3.0)	2.5 (2.0, 3.4)	0.377
TT (S)	17.9 (17.0, 18.8)	17.7 (17.1, 18.5)	0.527
AFP (ng/mL)	66.1 (3.9, 2696.0)	33.2 (4.1, 437.9)	0.084
Maximum diameter(mm)	42 (27.0, 66.0)	45.5 (32.3, 70.8)	0.159
Subtype			0.870
MTM-HCC	36 (24.5%)	15 (23.4%)	
Non-MTM-HCC	111 (75.5%)	49 (76.6%)	

Notes: Quantitative data are expressed as mean ± standard deviation when normally distributed, and as median (interquartile range) when not normally distributed. Qualitative data are expressed as numbers (percentages).
Abbreviations: MTM-HCC, macrotrabecular-massive hepatocellular carcinoma; AFP, alpha-fetoprotein; AST, aspartate aminotransferase; ALT, alanine aminotransferase; ALB, albumin; GLO, globulin; A/G, albumin-globulin ratio; TBIL, total bilirubin; DBIL, direct bilirubin; IBIL, indirect bilirubin; ALP, alkaline phosphatase; CREA, creatinine; APTT, activated partial thromboplastin time; PTA, prothrombin activity; PT, prothrombin time; FIB, fibrinogen; TT, thrombin time.

Table 2 Univariate Analysis of Preoperative Data for MTM-HCC and Non-MTM-HCC Patients

Characteristic	MTM-HCC (n=51)	Non-MTM-HCC (n=160)	*P* Value
Gender			0.038
Male	46(90.2%)	123 (76.9%)	
Female	5 (9.8%)	37 (23.1%)	
Age (years)	54.86 (±8.11)	58.16 (±10.49)	0.058
HbsAg/HCV Ab			0.33
Positive	39 (76.5%)	111 (69.4%)	
Negative	12 (23.5%)	49 (30.6%)	
Cirrhosis			0.885
Yes	40 (78.4%)	127 (79.4%)	
No	11 (21.6%)	33 (20.6%)	
Splenomegaly			0.056
Yes	18 (35.3%)	81 (50.6%)	
No	33 (64.7%)	79 (49.4%)	
Ascites			0.078
Yes	4 (7.8%)	29 (18.1%)	
No	47 (92.2%)	131 (81.9%)	
Portal hypertension			0.569
Yes	20 (39.2%)	70 (43.8%)	
No	31 (60.8%)	90 (56.2%)	

(*Continued*)

Table 2 (Continued).

Characteristic	MTM-HCC (n=51)	Non-MTM-HCC (n=160)	*P* Value
ALT (U/L)			0.017
<40	26 (51.0%)	111 (69.4%)	
≥40	25 (49.0%)	49 (30.6%)	
AST (U/L)			<0.001
<35	17 (33.3%)	96 (60.0%)	
≥35	34 (66.7%)	64 (40.0%)	
ALB (g/L)	40.9 (36.9, 43.2)	39.4 (36.35, 42.5)	0.267
GLO (g/L)	27.5 (25.3, 31.0)	27.3 (24.2, 31.2)	0.454
A/G	1.4 (1.3, 1.6)	1.5 (1.2, 1.7)	0.901
TB (umol/L)	12.4 (9.4, 18.4)	13.1 (9.1, 18.6)	0.947
DB (umol/L)	4.1 (3.1, 6.3)	4.0 (3.1, 5.6)	0.635
IB (umol/L)	8.6 (6.2, 11.6)	9.0 (6.0, 13.0)	0.829
ALP (U/L)	84.9 (71.5, 111.6)	84.5 (67.6, 107.9)	0.608
CREA (umol/L)	63.0 (56.0, 71.0)	62.0 (53.0, 71.9)	0.542
PT (S)	12.2 (11.6, 13.0)	12.4 (11.8, 13.0)	0.088
PTA (%)	95.2 (88.6, 100.2)	91.75 (86.9, 98.0)	0.093
APTT (S)	26.7 (25.7, 28.7)	27.5 (26.0, 29.6)	0.055
FIB (g/L)	2.7 (2.1, 3.6)	2.4 (2.0, 3.0)	0.097
TT (S)	17.7 (17.0, 18.3)	17.9 (17.1, 18.8)	0.241
AFP (ng/mL)			0.005
<400	28 (54.9%)	121 (75.6%)	
≥400	23 (45.1%)	39 (24.4%)	
Maximum diameter(mm)	55.0 (39.0, 83.0)	38.5 (27.0, 61.8)	<0.001

Notes: Quantitative data are expressed as mean ± standard deviation when normally distributed, and as median (interquartile range) when not normally distributed. Qualitative data are expressed as numbers (percentages).

Abbreviations: MTM-HCC, macrotrabecular-massive hepatocellular carcinoma; AFP, alpha-fetoprotein; AST, aspartate aminotransferase; ALT, alanine aminotransferase; ALB, albumin; GLO, globulin; A/G, albumin-globulin ratio; TBIL, total bilirubin; DBIL, direct bilirubin; IBIL, indirect bilirubin; ALP, alkaline phosphatase; CREA, creatinine; APTT, activated partial thromboplastin time; PTA, prothrombin activity; PT, prothrombin time; FIB, fibrinogen; TT, thrombin time.

Table 3 Multifactorial Analysis of Predicting MTM-HCC

Characteristic	Multivariable Logistic Regression Analysis	
	OR (95% CI)	*P* Value
ALT (≥40)	0.817 (0.331, 2.014)	0.660
AFP (≥400)	2.218 (1.077, 4.567)	0.031
AST (≥35)	2.728 (1.103, 6.749)	0.030
Gender	0.413 (0.144, 1.183)	0.099
Maximum diameter(mm)	1.013 (1.001, 1.025)	0.034

Abbreviations: AFP, alpha-fetoprotein; AST, aspartate aminotransferase; ALT, alanine aminotransferase; OR, odds ratio; CI, confidence interval.

Feature Extraction and Selection

A total of 1409 features were extracted from the patients' original and derived ultrasound images. First, 260 features with ICC lower than 0.8 were excluded after intraobserver agreement analysis; variance filtering and mutual information method were used to exclude 16 features with zero variance and 423 features with zero MIC; and 690 features were excluded by embedding method combined with XGBoost. Twenty features with non-zero coefficients were ultimately identified (Supplementary Figures 1 and 2).

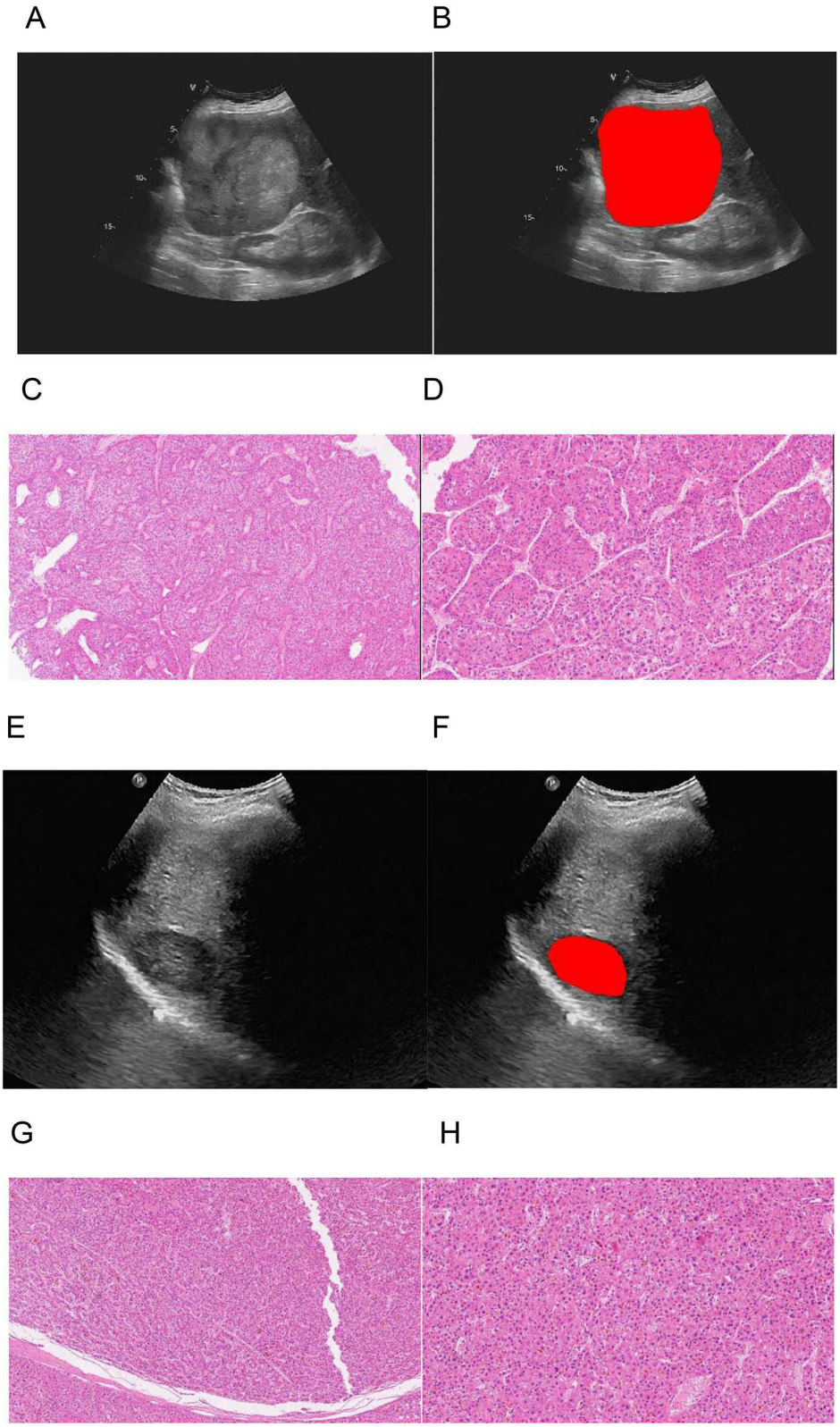

Figure 4 The ultrasound images and histological patterns of non-MTM-HCC and MTM-HCC. (**A**)–(**D**): Ultrasound and pathological images of a 65-year-old male patient with MTM-HCC; (**A**) and (**B**) Ultrasound images of MTM-HCC patients and ROIs; (**C**) and (**D**): Histopathology images of MTM-HCC at low and medium magnification; (**E**)–(**H**) Ultrasound and pathological images of a 70-year-old male patient with non-MTM-HCC; (**E**) and (**F**) Ultrasound images of non-MTM-HCC patients and ROIs; (**G**) and (**H**): Histopathology images of non-MTM-HCC at low and medium magnification.

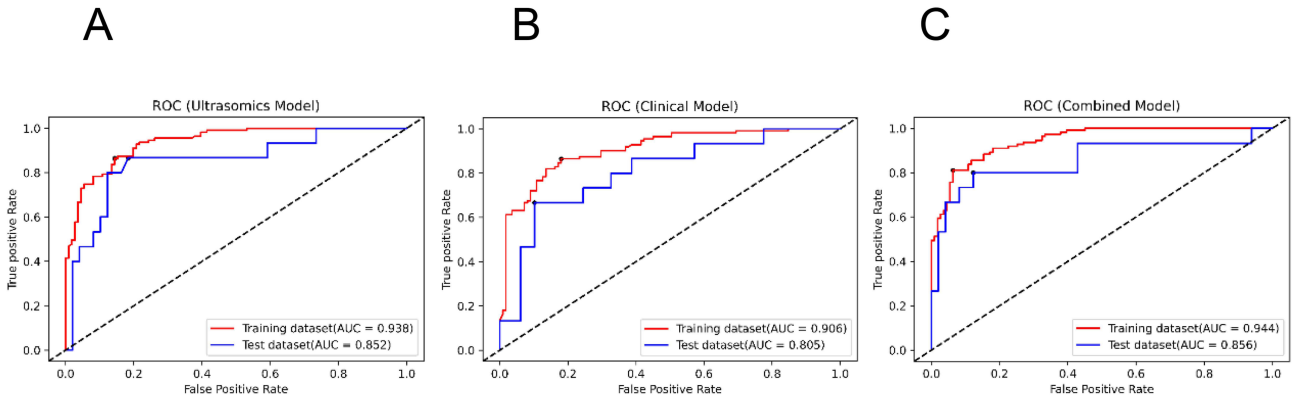

Figure 5 ROC curves in RF training set and test set. (**A**) ROC curves of ultrasomics model based on the ultrasound image features. (**B**) ROC curves of clinical model based on clinical data. (**C**) ROC curves of combined model based on clinical data and ultrasomics features.

Performance of the Clinical, Ultrasomics, and Combined Models

Comparing the five ML algorithms, the AUCs of the clinical, ultrasomics, and combined models in the test set were 0.805, 0.852, 0.856; 0.621, 0.822, 0.841; 0.733, 0.701, 0.852; 0.639, 0.812, 0.825; 0.743, 0.771, 0.860; the accuracies were 0.750, 0.859, 0.859; 0.672, 0.734, 0.813; 0.656, 0.719, 0.734; 0.625, 0.797, 0.766; 0.688, 0.703, 0.750; the sensitivities were 0.733, 0.800, 0.800; 0.733, 0.800, 0.733; 0.667, 0.733, 0.733; 0.667, 0.733, 0.800; 0.867, 0.733, 0.733; and the specificities were 0.755, 0.878, 0.878; 0.653, 0.714, 0.837; 0.653, 0.714, 0.735; 0.612, 0.816, 0.755; 0.633, 0.694, 0.755, respectively. The results showed that the combined models had higher AUCs than the clinical and ultrasomics models built using the five algorithms. Similarly, the ultrasomics model had a higher AUC than the clinical model constructed with RF, XGBoost, DT, and LR. The RF-based combined model and ultrasomics model (AUC of 0.856 and 0.852, respectively) and the LR-based combined model (AUC of 0.860) had higher AUC values. However, The RF-based models exhibited higher accuracy and specificity compared to models constructed using the other four algorithms. Among the three RF-based models, AUC, accuracy, sensitivity, and specificity were higher for the combined model and ultrasound model than for the clinical model. Furthermore, the combined model demonstrated higher AUC and similar accuracy, sensitivity, and specificity compared to the ultrasomics model. Taken together, all five ML-based ultrasomics models were effective in distinguishing MTM-HCC from non-MTM-HCC, and the combined models exhibited superior performance than the clinical and ultrasomics models. Additionally, RF-based models had the best overall performance compared to other ML-based models.

The ROC curves for the three RF-based models are shown in Figure 5, and the results of the models constructed using the five algorithms are shown in Table 4.

Table 4 Prediction Results of Different Models for Training Set and Test Set

Algorithms	Dataset	Model	Accuracy (%)	Sensitivity (%)	Specificity (%)	AUC (95%CI)	*P* Value
RF	Training set	Clinical	83.78	85.59	81.98	0.906(0.859–0.941)	<0.0001
		Ultrasomics	85.59	90.99	80.18	0.938(0.898–0.966)	<0.0001
		Combined	86.04	89.19	82.88	0.944(0.905–0.970)	<0.0001
	Test set	Clinical	75.00	73.33	75.51	0.805(0.687–0.894)	<0.0001
		Ultrasomics	85.94	80.00	87.76	0.852(0.741–0.929)	<0.0001
		Combined	85.93	80.00	87.76	0.856(0.746–0.931)	<0.0001
	Training set	Clinical	88.29	93.69	82.88	0.952(0.916–0.976)	<0.0001
		Ultrasomics	87.84	90.09	85.59	0.958(0.923–0.981)	<0.0001

(*Continued*)

Table 4 (Continued).

Algorithms	Dataset	Model	Accuracy (%)	Sensitivity (%)	Specificity (%)	AUC (95%CI)	*P* Value
XGBoost		Combined	88.29	92.79	83.78	0.963(0.930–0.984)	<0.0001
	Test set	Clinical	67.19	73.33	65.31	0.621(0.491–0.739)	0.1420
		Ultrasomics	73.44	80.00	71.43	0.822(0.706–0.906)	<0.0001
		Combined	81.25	73.33	83.67	0.841(0.728–0.920)	<0.0001
	Training set	Clinical	77.03	72.97	81.08	0.861(0.808–0.904)	<0.0001
		Ultrasomics	83.33	92.79	73.87	0.896(0.848–0.933)	<0.0001
SVM		Combined	78.83	80.18	77.48	0.854(0.800–0.897)	<0.0001
	Test set	Clinical	65.63	66.67	65.31	0.733(0.608–0.836)	0.0005
		Ultrasomics	71.88	73.33	71.43	0.701(0.573–0.809)	0.0283
		Combined	73.44	73.33	73.47	0.852(0.741–0.928)	<0.0001
	Training set	Clinical	99.10	99.10	99.10	0.997(0.978–1.000)	<0.0001
		Ultrasomics	84.23	84.68	83.78	0.894(0.846–0.931)	<0.0001
DT		Combined	90.99	99.10	82.88	0.951(0.914–0.976)	<0.0001
	Test set	Clinical	62.50	66.67	61.22	0.639(0.509–0.755)	0.074
		Ultrasomics	79.69	73.33	81.63	0.812(0.694–0.898)	<0.0001
		Combined	76.56	80.00	75.51	0.825(0.710–0.909)	<0.0001
	Training set	Clinical	74.32	72.97	75.68	0.831(0.775–0.878)	<0.0001
		Ultrasomics	74.77	82.88	66.67	0.781(0.721–0.834)	<0.0001
LR		Combined	77.93	80.18	75.68	0.870(0.818–0.911)	<0.0001
	Test set	Clinical	68.75	86.67	63.27	0.743(0.618–0.844)	0.0001
		Ultrasomics	70.31	73.33	69.39	0.771(0.649–0.867)	0.0002
		Combined	75.00	73.33	75.51	0.860(0.750–0.934)	<0.0001

Abbreviations: RF, random forest; XGBoost, eXtreme gradient boosting; SVM, support vector machine; DT decision tree; LR, logistic regression; AUC, area under the receiver operating characteristic curve.

Discussion

MTM-HCC is a new histological subtype of HCC identified by the WHO in 2019. Compared to non-MTM-HCC, MTM-HCC is associated with a larger tumor volume, elevated preoperative AFP levels, vascular invasion, higher Edmondson-Steiner grade,[18,25,27] and greater invasiveness and metastatic potential. It is an independent predictor for early post-operative recurrence. Studies have shown that MTM-HCC may benefit from neoadjuvant therapy.[11,18,28] However, MTM-HCC can only be diagnosed by postoperative histopathology or invasive preoperative biopsy, limiting the treatment options for patients with this HCC subtype. Therefore, accurate preoperative predictions using non-invasive and effective methods are crucial for guiding optimal personalized treatment plans.

Radiomics is an emerging non-invasive technique that effectively mines image information. In this study, we extracted 1409 ultrasound image features from the original and derived images of each patient, and performed feature dimensionality reduction through a combination of ICC, variance filtering, mutual information, and the embedding method combined with XGBoost. We identified 20 best features and constructed models using RF, XGBoost, SVM, DT, and LR for the preoperative prediction of MTM-HCC. Analysis showed that all five ML-based ultrasomics models effectively predicted MTM-HCC and the combined models had superior predictive performance than the clinical and ultrasomics models. In addition, RF-based models exhibited better overall performance than models constructed using the other four algorithms. The RF-based combined and ultrasomics models had significantly higher AUCs (0.856 and 0.852 vs 0.805), accuracies (0.859 and 0.859 vs 0.750), specificities (0.878 and 0.878 vs 0.755), and sensitivities (0.800 and 0.800 vs 0.733) than the RF-based clinical model. Furthermore, AUC was slightly higher for the combined model compared to the ultrasomics model. Our results indicated that non-invasive ultrasomics is effective for predicting MTM-HCC, highlighting its potential clinical value.

Previous studies have reported that MRI and CT image features are useful for predicting MTM-HCC.[18–20,29–32] Zhang et al[20] found that the AUC of the MRI radiomics model based on the LR algorithm was 0.766 and 0.739, and the

specificities were 0.847 and 0.804, respectively. In a multicentre study, Li et al constructed a DL-based dual-energy CT radiomics nomogram based on deep learning (DL) features and manual features. Their model has an AUC of 0.91 in the training set, 0.87 in the internal test set, and 0.89 in the external test set.[19] Our study revealed that the RF-based ultrasomics model had an AUC of 0.938 in the training set and 0.852 in the test set, demonstrating favorable predictive performance. This also indicates that compared with CT and MRI, ultrasomics model features can also provide more information for predicting MTM-HCC. Among the features of constructing ultrasonic models, "Glszone Variance" and "Gldm_Small Dependence High Gray Level Emphasis" had the highest feature coefficients, describing the heterogeneity of texture features in MTM-HCC. It is consistent with some imaging features extracted from previous studies of HCC.[20] The abundance of information in grayscale ultrasound images, combined with the radiation-free, simple, and cost-effective characteristics offer significant potential for predicting MTM-HCC.

We found that MTM-HCC patients had higher AST levels than non-MTM-HCC patients ($P < 0.05$). Shan et al found that higher AST levels were associated with lower survival.[33] The increased release of AST may be attributed to extensive necrosis within the MTM-HCC tumor.

There are also some limitations in this study. The study included only retrospective cases from one hospital, and the sample size of the data was limited, lacking external test sets. As a result, the stability and applicability of the established prediction models could not be fully validated. Therefore, further international multicenter studies are warranted to enhance the effectiveness and generalizability of the model.

Conclusion

In conclusion, the ultrasomics model can distinguish the MTM-HCC subtype through machine learning. The random forest machine learning method has the best comprehensive performance and excellent prediction ability, which will provide a new method for non-invasive identification of MTM-HCC.

Abbreviations

ML, machine learning; MTM-HCC, macrotrabecular-massive hepatocellular carcinoma; RF, random forest; XGBoost, eXtreme gradient boosting; SVM, support vector machine; DT,decision tree; LR, logistic regression; AUC, area under the receiver operating characteristic curve; AFP, alpha-fetoprotein; AST, aspartate aminotransferase; ALT, alanine aminotransferase; ALB, albumin; GLO, globulin; A/G, albumin-globulin ratio; TBIL, total bilirubin; DBIL, direct bilirubin; IBIL, indirect bilirubin; ALP, alkaline phosphatase; CREA, creatinine; APTT, activated partial thromboplastin time; PTA, prothrombin activity; PT, prothrombin time; FIB, fibrinogen; TT, thrombin time.

Ethics Statement

This retrospective study was reviewed and approved by the Hospital Ethics Committee of Henan Provincial People's Hospital. The study was conducted in accordance with the Declaration of Helsinki and all patient data were treated confidentially. Given the retrospective observational nature of the study, the Institutional Review Board waived the requirement for written informed consent from patients.

Acknowledgments

Thank all the staff authors for their contributions to this study.

Funding

The author(s) declare financial support was received for the research, authorship, and/or publication of this article. This study was sponsored by the National Natural Science Foundation of China (grant no. 82371987), the Key Research and Development Program of Henan Province (no. 221111310400), the Henan Rehabilitation Clinical Medical Research Center and Medical Appropriate Technology Promotion Project of Henan Province (no. SYJS2022018), and the Science and Technology Breakthrough Plan Project of Henan Province (no. 242102311104).

Disclosure

The authors declare that the research was conducted in the absence of any commercial or financial relationships that could be construed as a potential conflict of interest.

References

1. Bray F, Laversanne M, Sung H, et al. Global cancer statistics 2022: GLOBOCAN estimates of incidence and mortality worldwide for 36 cancers in 185 countries. *Ca a Cancer J Clinicians*. 2024;74(3):229–263. doi:10.3322/caac.21834
2. Yang JD, Hainaut P, Gores GJ, et al. A global view of hepatocellular carcinoma: trends, risk, prevention and management. *Nat Rev Gastroenterol Hepatol*. 2019;16(10):589–604. doi:10.1038/s41575-019-0186-y
3. Chu LC, Fishman EK. AI as Virtual Biopsy Tool to Predict Macrotrabecular-Massive Hepatocellular Carcinoma. *Radiology*. 2023;308(2):e231663. doi:10.1148/radiol.231663
4. Nagtegaal ID, Odze RD, Klimstra D, et al. The 2019 WHO classification of tumours of the digestive system. *Histopathology*. 2020;76(2):182–188. doi:10.1111/his.13975
5. Calderaro J, Ziol M, Paradis V, et al. Molecular and histological correlations in liver cancer. *J Hepatol*. 2019;71(3):616–630. doi:10.1016/j.jhep.2019.06.001
6. Loy LM, Low HM, Choi JY, et al. Variant Hepatocellular Carcinoma Subtypes According to the 2019 WHO Classification: an Imaging-Focused Review. *Am J Roentgenol*. 2022;219(2):212–223. doi:10.2214/AJR.21.26982
7. Katabathina VS, Khanna L, Surabhi VR, et al. Morphomolecular Classification Update on Hepatocellular Adenoma, Hepatocellular Carcinoma, and Intrahepatic Cholangiocarcinoma. *RadioGraphics*. 2022;42(5):1338–1357. doi:10.1148/rg.210206
8. Calderaro J, Couchy G, Imbeaud S, et al. Histological subtypes of hepatocellular carcinoma are related to gene mutations and molecular tumour classification. *J Hepatol*. 2017;67(4):727–738. doi:10.1016/j.jhep.2017.05.014
9. Jeon Y, Benedict M, Taddei T, et al. Macrotrabecular Hepatocellular Carcinoma: an Aggressive Subtype of Hepatocellular Carcinoma. *Am J Surg Pathol*. 2019;43(7):943–948. doi:10.1097/PAS.0000000000001289
10. Matsuura T, Ueda Y, Harada Y, et al. Histological diagnosis of polyploidy discriminates an aggressive subset of hepatocellular carcinomas with poor prognosis. *Br J Cancer*. 2023;129(8):1251–1260. doi:10.1038/s41416-023-02408-6
11. Liu LL, Zhang SW, Chao X, et al. Coexpression of CMTM6 and PD-L1 as a predictor of poor prognosis in macrotrabecular-massive hepatocellular carcinoma. *Cancer Immunol Immunother*. 2021;70(2):417–429. doi:10.1007/s00262-020-02691-9
12. Hawkins S, Wang H, Liu Y, et al. Predicting malignant nodules from screening CTs. *J Thoracic Oncol*. 2016;11(12):2120. doi:10.1016/j.jtho.2016.07.002
13. Xie T, Gong J, Zhao Q, et al. Development and validation of peritumoral vascular and intratumoral radiomics to predict pathologic complete responses to neoadjuvant chemotherapy in patients with triple-negative breast cancer. *BMC Med Imaging*. 2024;24(1):136. doi:10.1186/s12880-024-01311-7
14. Ji GW, Zhu FP, Xu Q, et al. Radiomic Features at Contrast-enhanced CT Predict Recurrence in Early Stage Hepatocellular Carcinoma: a Multi-Institutional Study. *Radiology*. 2020;294(3):568–579. doi:10.1148/radiol.2020191470
15. Gillies RJ, Kinahan PE, Hricak H. Radiomics: images Are More than Pictures, They Are Data. *Radiology*. 2016;278(2):563–577. doi:10.1148/radiol.2015151169
16. Bera K, Braman N, Gupta A, et al. Predicting cancer outcomes with radiomics and artificial intelligence in radiology. *Nat Rev Clin Oncol*. 2022;19(2):132–146. doi:10.1038/s41571-021-00560-7
17. Liu F, Liu D, Wang K, et al. Deep Learning Radiomics Based on Contrast-Enhanced Ultrasound Might Optimize Curative Treatments for Very-Early or Early-Stage Hepatocellular Carcinoma Patients. *Liver Cancer*. 2020;9(4):397–413. doi:10.1159/000505694
18. Feng Z, Li H, Liu Q, et al. CT Radiomics to Predict Macrotrabecular-Massive Subtype and Immune Status in Hepatocellular Carcinoma. *Radiology*. 2023;307(1):e221291. doi:10.1148/radiol.221291
19. Li M, Fan Y, You H, et al. Dual-Energy CT Deep Learning Radiomics to Predict Macrotrabecular-Massive Hepatocellular Carcinoma. *Radiology*. 2023;308(2):e230255. doi:10.1148/radiol.230255
20. Zhang Y, He D, Liu J, et al. Preoperative prediction of macrotrabecular-massive hepatocellular carcinoma through dynamic contrast-enhanced magnetic resonance imaging-based radiomics. *World J Gastroenterol*. 2023;29(13):2001–2014. doi:10.3748/wjg.v29.i13.2001
21. Akkus Z, Cai J, Boonrod A, et al. A Survey of Deep-Learning Applications in Ultrasound: artificial Intelligence-Powered Ultrasound for Improving Clinical Workflow. *JACR*. 2019;16(9 Pt B):1318–1328. doi:10.1016/j.jacr.2019.06.004
22. Peng Y, Lin P, Wu L, et al. Ultrasound-Based Radiomics Analysis for Preoperatively Predicting Different Histopathological Subtypes of Primary Liver Cancer. *Front Oncol*. 2020;10:1646. doi:10.3389/fonc.2020.01646
23. Ren S, Qi Q, Liu S, et al. Preoperative prediction of pathological grading of hepatocellular carcinoma using machine learning-based ultrasomics: a multicenter study. *Eur J Radiol*. 2021;143:109891. doi:10.1016/j.ejrad.2021.109891
24. Dong Y, Zhou L, Xia W, et al. Preoperative Prediction of Microvascular Invasion in Hepatocellular Carcinoma: initial Application of a Radiomic Algorithm Based on Grayscale Ultrasound Images. *Front Oncol*. 2020;10:353. doi:10.3389/fonc.2020.00353
25. Ziol M, Poté N, Amaddeo G, et al. Macrotrabecular-massive hepatocellular carcinoma: a distinctive histological subtype with clinical relevance. *Hepatology*. 2018;68(1):103–112. doi:10.1002/hep.29762
26. Bektas CT, Kocak B, Yardimci AH, et al. Clear Cell Renal Cell Carcinoma: machine Learning-Based Quantitative Computed Tomography Texture Analysis for Prediction of Fuhrman Nuclear Grade. *Eur Radiol*. 2019;29(3):1153–1163. doi:10.1007/s00330-018-5698-2
27. Fuster-Anglada C, Mauro E, Ferrer-Fàbrega J, et al. Histological predictors of aggressive recurrence of hepatocellular carcinoma after liver resection. *J Hepatol*. 2024;81(6):S0168–8278(24)02324–9. doi:10.1016/j.jhep.2024.06.018
28. Sessa A, Mulé S, Brustia R, et al. Macrotrabecular-Massive Hepatocellular Carcinoma: light and Shadow in Current Knowledge. *J Hepatocell Carcinoma*. 2022;9:661–670. doi:10.2147/JHC.S364703
29. Gong Q, Zhang Y, Wu T, et al. Comparison of computed tomography and magnetic resonance imaging findings and histopathological features of macrotrabecular-massive hepatocellular carcinoma. *Quant Imag Med Surg*. 2023;13(7):4633–4640. doi:10.21037/qims-22-940

30. Rhee H, Cho ES, Nahm JH, et al. Gadoxetic acid-enhanced MRI of macrotrabecular-massive hepatocellular carcinoma and its prognostic implications. *J Hepatol*. 2021;74(1):109–121. doi:10.1016/j.jhep.2020.08.013
31. Kim TH, Woo S, Lee DH, et al. MRI imaging features for predicting macrotrabecular-massive subtype hepatocellular carcinoma: a systematic review and meta-analysis. *Eur Radiol*. 2024;34(10):6896–6907. doi:10.1007/s00330-024-10671-1
32. Cheng J, Li X, Wang L, et al. Evaluation and Prognostication of Gd-EOB-DTPA MRI and CT in Patients With Macrotrabecular-Massive Hepatocellular Carcinoma. *J Magn Reson Imaging*. 2024;59(6):2071–2081. doi:10.1002/jmri.29052
33. Shan Y, Yu X, Yang Y, et al. Nomogram for the Preoperative Prediction of the Macrotrabecular-Massive Subtype of Hepatocellular Carcinoma. *J Hepatocell Carcinoma*. 2022;9:717–728. doi:10.2147/JHC.S373960